

# Design, construction and characterization of a prompt gamma activation analysis facility at the Oregon State University TRIGA<sup>®</sup> reactor

Joshua A. Robinson · Michael R. Hartman ·  
Steven R. Reese

Received: 19 June 2009 / Published online: 10 September 2009  
© Akadémiai Kiadó, Budapest, Hungary 2009

**Abstract** A prompt gamma neutron activation analysis facility has been designed, built, and characterized at the Oregon State University TRIGA<sup>®</sup> reactor. This facility was designed for versatile multi-elemental analyses. The facility utilizes the leakage neutrons originating from beam port #4 of the Oregon State University TRIGA<sup>®</sup> reactor. The neutrons are collimated through a series of lead and Boral<sup>®</sup> collimators, and filtered through both a bismuth filter and single-crystal sapphire. Samples are irradiated in a sample chamber outside the biological shielding of the reactor, and the resulting gamma radiation produced from neutron interactions within the sample is monitored using a high-purity germanium detector (HPGe). The thermal and epithermal neutron fluxes were measured using gold-foil irradiations and found to be  $2.81 \times 10^7$  and  $1.70 \times 10^4 \text{ cm}^{-2} \text{ s}^{-1}$ , respectively. The resulting cadmium ratio was 106. Measured detection limits for boron, chlorine, and potassium in a NIST SRM 1571 orchard leaf were  $5.6 \times 10^{-4} \text{ mg/g}$ ,  $8.2 \times 10^{-2} \text{ mg/g}$ , and  $1.0 \text{ mg/g}$ , respectively. Detection limits for additional elements and samples are presented.

**Keywords** Prompt gamma neutron activation analysis · Research reactor · Non-destructive analysis · Elemental analysis

## Introduction

To expand the experimental capabilities of the Oregon State University TRIGA<sup>®</sup> Reactor (OSTR), a facility for prompt gamma neutron activation analysis (PGNAA) has been constructed. PGNAA is a nondestructive means of conducting elemental analysis on materials through neutron capture interactions. These neutron capture reactions produce compound nuclei in an excited state, which de-excite almost instantaneously through the emission of discrete-energy gamma-rays. The energy spectrum of the gamma-rays is characteristic of the emitting nuclide, and the number of gamma rays at a specific energy is directly proportional to the quantity of the emitting element. There are in principle at least 80 elements, which can be measured using PGNAA [1]. These include elements such as B, H, Cd, and Gd, which are difficult or impossible to detect using instrumental neutron activation analysis (INAA).

Facilities for PGNAA have been implemented at a number of research reactors around the world. Among some of the best are the state-of-the-art facilities at the National Institute of Standards and Technology (NIST) [2], Budapest [3], and the University of Texas [4]. Information on additional facilities can be found in the PGNAA Hand Book [5].

Prompt gamma neutron activation analysis has many advantages over other elemental analysis techniques because of its nondestructive nature and flexibility, as well as allowing for the analysis of many elements which do not produce sufficient amounts of activity to be practically

---

J. A. Robinson (✉)  
Department of Nuclear Engineering and Radiation Health  
Physics, Oregon State University, Corvallis, OR 97331-5903,  
USA  
e-mail: robinjos@onid.orst.edu

M. R. Hartman  
Department of Nuclear Engineering and Radiological Sciences,  
University of Michigan, Ann Arbor, MI 48109-2104, USA

S. R. Reese  
Radiation Center, Oregon State University, Corvallis,  
OR 97331-5903, USA

measured using INAA. Also, with PGNAA large pieces of materials such as pottery can be analyzed, which would be too large to place in the reactor [6], extremely low levels of radioactivity are produced within the samples because of the relatively low integrated flux, the results are produced in real-time during the irradiation, and because of the nondestructive nature of PGNAA the samples can be recounted to obtain better statistics.

### OSTR reactor

The OSTR is a TRIGA<sup>®</sup> pool-type reactor cooled by natural convection and operates at 1 MW. The core of the reactor is surrounded by a graphite reflector and is located near the bottom of a water-filled aluminum tank. The reactor is equipped with four beam ports, which penetrate the reactor biological shield and reactor tank. Beam ports #1 and #2 are radial beam ports, which terminate at the outer edge of the graphite reflector. Beam port #3 is tangential to the outer edge of the core. Beam port #4 is a radial piercing beam port, which penetrates through the

graphite reflector and terminates at the outer edge of the reactor core, as illustrated in Fig. 1.

Of the four beam ports, beam port #4 was the only available beam port suitable for the PGNAA facility. As described above, beam port #4 is a piercing beam port, which looks directly at the core. The primary advantage of this beam port is that it has a very high thermal flux due to its orientation to the core. However, this also results in very large fast-neutron and gamma components as well. For the PGNAA facility, it was therefore important to include appropriate beam filtering to minimize the contribution of the fast-neutrons and gamma rays, while still maintaining a high thermal flux.

### Description and design of the facility

The main components of the OSTR PGNAA facility include a collimator, beam shutter, sample chamber, beam stop, and a high purity germanium (HPGe) detector housed inside a large gamma and neutron shield, as depicted in Fig. 2.

**Fig. 1** Horizontal section of the OSTR with the PGNAA facility, showing radial beam ports, and shielding configuration

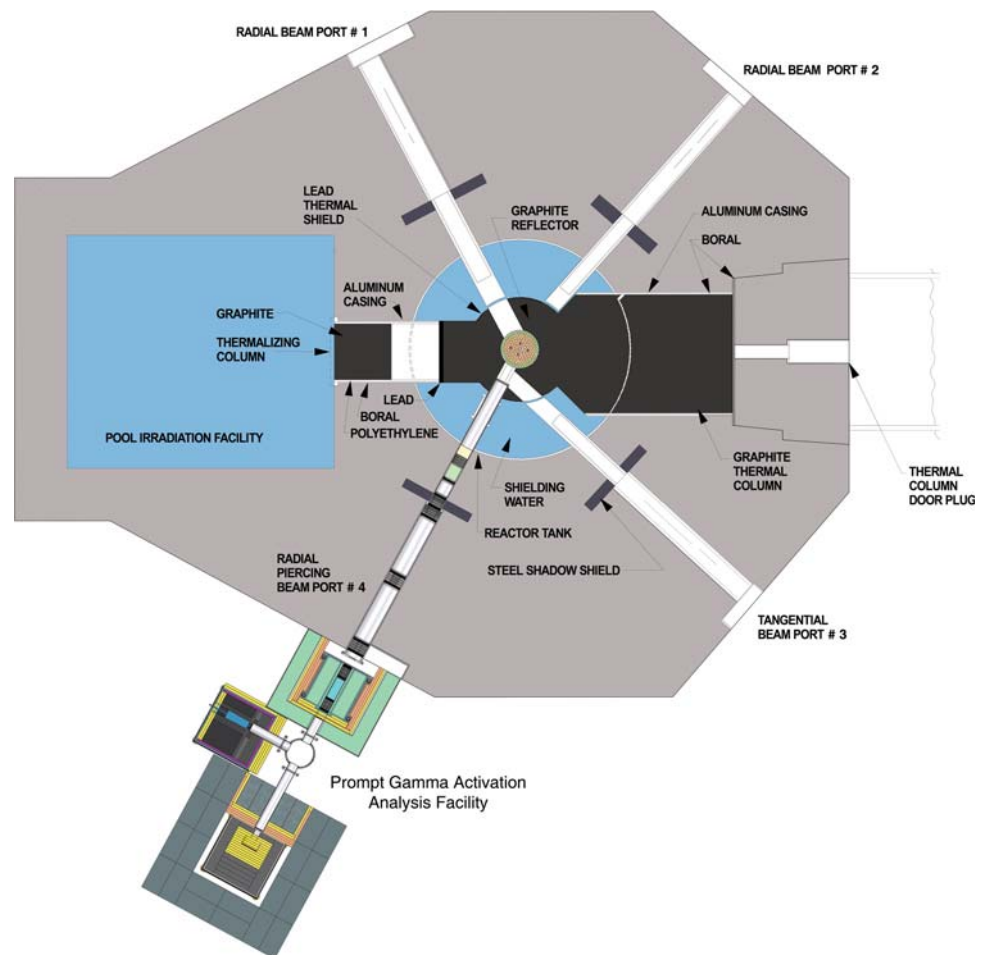


**Fig. 2** Schematic illustration of the PGNAA facility, showing the arrangement of the various components within the facility. (Note: the reactor biological shield surrounding the collimator has been omitted for clarity)

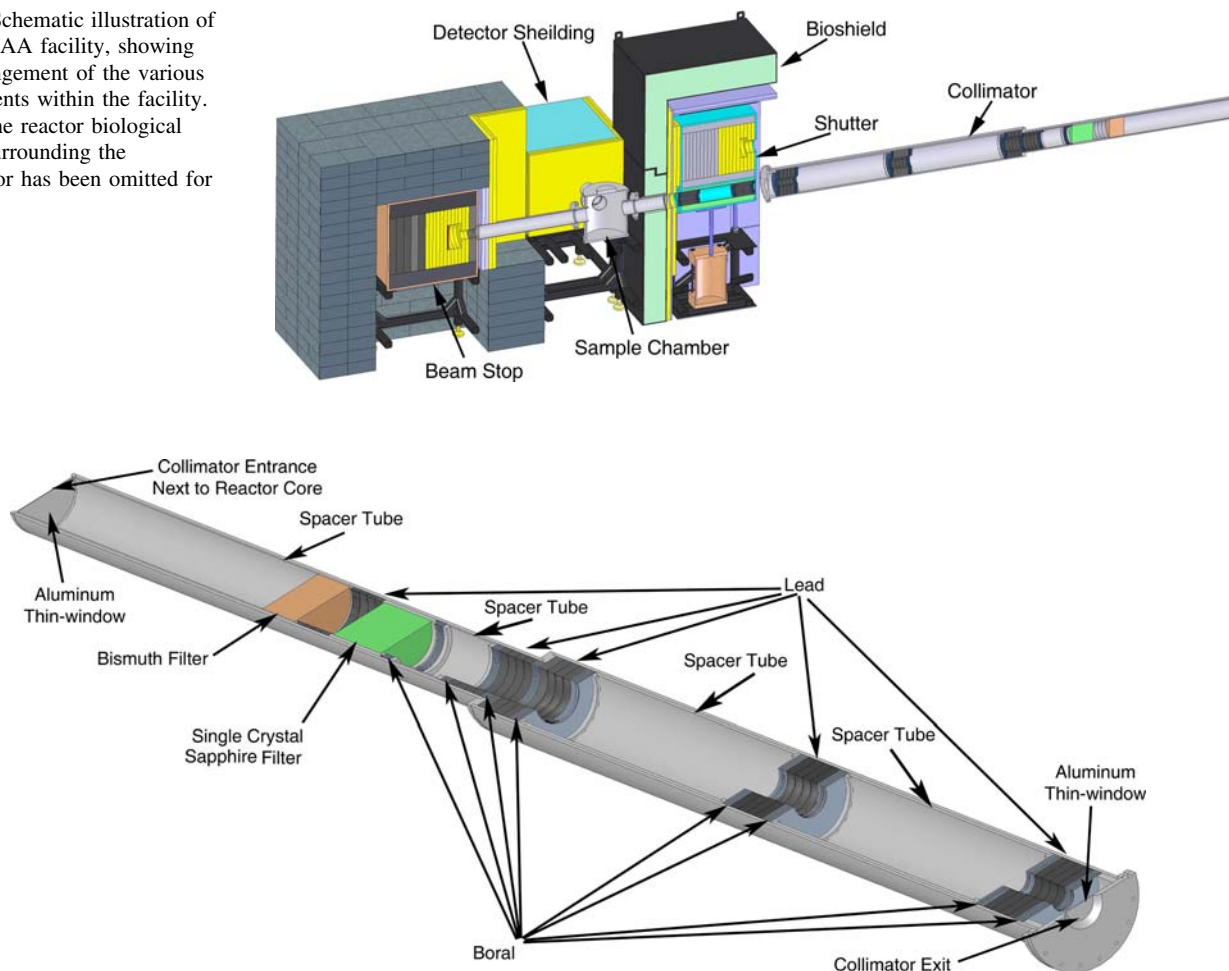


**Fig. 3** Cross-sectional illustration of the PGNAA collimator with internal components

### Collimator

The PGNAA collimator is installed in beam port #4 and was designed with the following objectives; reduce the fast neutron and gamma components of the beam, while still maintaining a high thermal neutron flux, and to collimate the neutron beam to a diameter of 2 cm located 1 m from the downstream end of the collimator. The shell of the collimator consists of welded schedule 40 aluminum pipes with aluminum thin-windows on either end. The thin-windows permit the collimator to be evacuated or filled with helium to reduce the attenuation of the neutron beam and the concomitant production of gamma rays from neutron interaction with air. The aluminum thin-window on the reactor side is welded in place while the aluminum thin-window on the exit side is bolted on with an o-ring sealed flange, allowing easy access to the materials within the collimator.

A series of lead and Boral<sup>®</sup> rings are used to collimate the neutron beam to a 2-cm uniform diameter within the

center of the beam at the sample location, and bismuth and sapphire filters serve to reduce the gamma and fast neutron component of the extracted neutron beam. A detailed cross-sectional view of the collimator is shown in Fig. 3.

A large-grain, poly-crystalline bismuth filter was used because of its large absorption cross section for gammas and its relatively good transmittance of thermal neutrons [7]. The bismuth in the collimator is 15 cm in diameter and 10.12 cm in length. It was made by melting bismuth in a cylindrical aluminum container at approximately 300 °C. After it was fully melted, the temperature was reduced to 250 °C, and was left in the oven for about 4 days to anneal. This was done to allow crystal growth during solidification. The bismuth was then removed from the oven and the top and bottom were machined off to remove any imperfections on either end.

The single crystal sapphire filter was used primarily to reduce the fast neutron component of the beam. Fast-neutrons are strongly attenuated by the sapphire due to scattering collisions from the highly energy dependent cross

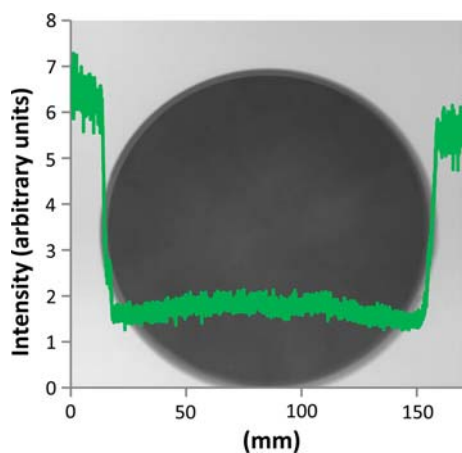


**Fig. 4** Bismuth radiographs taken in NRF, with line profile scan of intensity across horizontal midplane of image

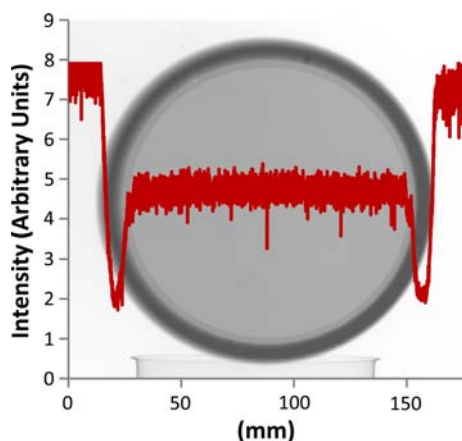


**Fig. 5** Sapphire radiographs taken in NRF, with line profile scan of intensity across horizontal midplane of image

section, which is low for thermal neutrons but strongly increases for epithermal and fast-neutrons[8, 9]. This filter is composed of three cylindrical-shaped, single-crystal sapphire pieces with 15 cm diameters and approximate lengths of 64, 46, and 40 mm. The crystals are oriented with the  $0001 \pm 30^\circ$  axis parallel to the incoming neutron beam.

Neutron radiograph images were taken in the OSTR neutron radiography facility (NRF) of both the bismuth and the sapphire filter to measure their thermal neutron transmission. The measured transmission for all three sapphire filters combined and the bismuth filter were  $66.05 \pm 0.14$  and  $27.98 \pm 0.06\%$ , respectively. The results from these radiographs are summarized in Figs. 4, 5, and Table 1.

#### Shutter

Following the collimator is a shutter, which acts as a movable beam stop for the neutron beam before it enters

**Table 1** Summary of sapphire and bismuth radiograph results

Crystal	Thickness (cm)	Transmittance (%)	Standard deviation (%)
Sapphire 1	6.4	80.39	0.22
Sapphire 2	4.6	90.08	0.23
Sapphire 3	4.0	92.39	0.19
Sapphire 1, 2, and 3	15.0	66.05	0.14
Bismuth	10.2	27.98	0.06
Bismuth and sapphire <sup>a</sup>		18.49	0.06

<sup>a</sup> Determined from combining results from sapphire and bismuth

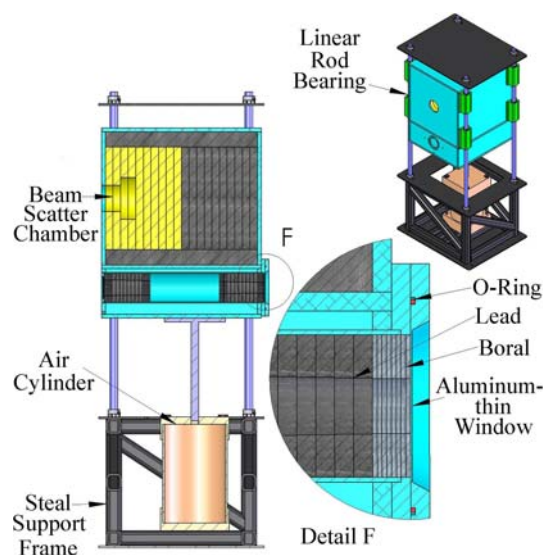


**Fig. 6** PGNAA shutter assembly

the sample chamber. The beam stop for the shutter consists of an aluminum box filled with lead and 5% borated polyethylene, and is mounted on an air cylinder with linear rod bearings for guides. To open the beam, air is applied to the cylinder and the beam stop is lifted out of position and the beam is aligned with an evacuated beam tube mounted under the beam stop. When the cylinder is vented, the beam stop falls to its closed position due to gravity alone. The advantage of this design is that it can be closed in the event of a loss of power and there are no mechanical components that are likely to fail which could leave the shutter in an open or intermediate position. A schematic diagram of this shutter is shown in Fig. 6. It is important to note that in addition to the main collimator, lead and Boral<sup>®</sup> collimators were extended into the beam tube in the shutter. The shutter is also surrounded by a biological shield, which serves to reduce the background radiation levels around the facility both when the shutter is open and when it is closed.

### Sample chamber and sample holder

The sample chamber was made of aluminum with an inside diameter of approximately 30 cm and a length of 33 cm. Both ends are equipped with aluminum plates machined such that they are partially recessed into the sample chamber. A vacuum tight seal is accomplished by o-rings, which are seated in both ends of the sample chamber. The detector is situated 90° to the incoming beam. Aluminum tubes are bolted onto the sample chamber to provide an evacuated flight path from the sample to the detector, as well as evacuated beam tubes for the neutron beam.

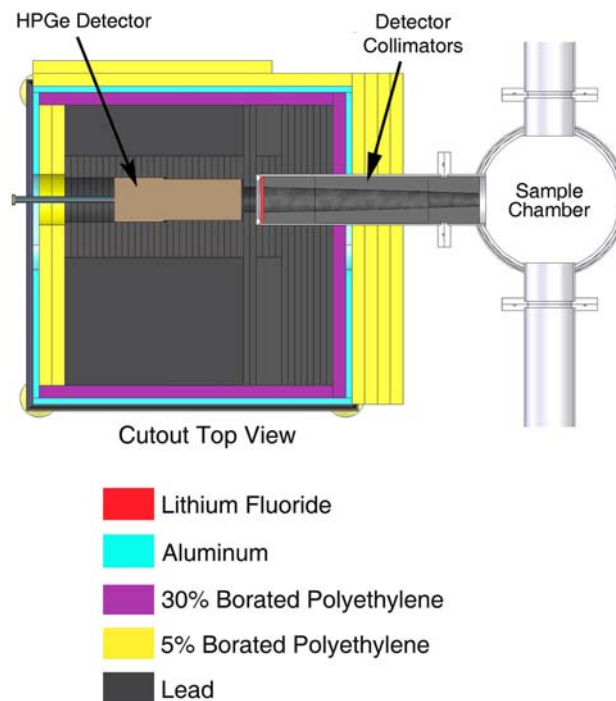
The sample holder, which is mounted inside the sample chamber, is designed to hold the sample in the beam while minimizing the interaction of the beam with the sample holder itself. This is accomplished by a rectangular shaped aluminum U machined out of a piece of approximately 0.6-cm thick aluminum plate whose posts are positioned on either side of the beam and situated such that the sample is held at a 45° angle to the beam. This positions the posts out of line of sight of the detector and minimizes self shielding for thin disk shaped samples. The sample holder is held in place by a vertical aluminum post with two aluminum pegs on one side and a piece of spring steel on the other side. This system allows for easy removal of the holder, which is necessary for precise and repeatable positioning of the samples on the holder. This system can be seen in Fig. 7.

### Detector and detector shielding

A HPGe detector with a resolution of 1.73 keV and a relative efficiency of 36.50% at 1.33 MeV is utilized for this facility. The sample to detector distance can be varied, and is nominally 60 cm. The detector is surrounded by a large amount of gamma and neutron shielding. The shielding was all carefully machined and supported inside a welded aluminum box. This configuration resulted in over 20 cm of lead on all sides except the side towards the shutter biological shield, which had 14 cm. There was

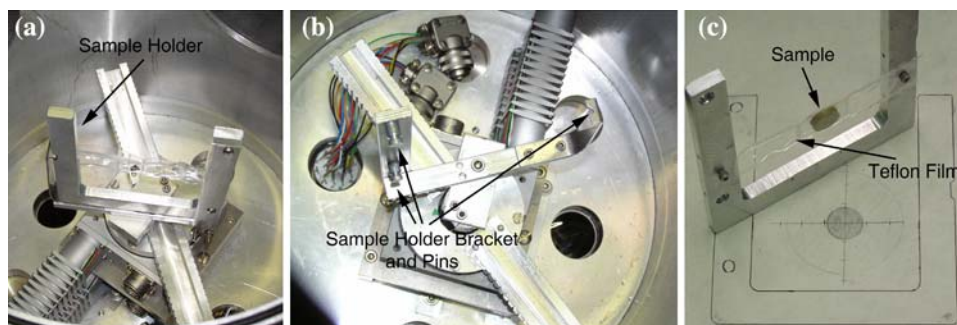
also 2.54–3.08 cm of borated polyethylene on all sides, and 12.7 cm of borated polyethylene on the front to account for the higher neutron flux coming from the beam line. Lead collimators were machined to fit inside the flight path between the sample and detector in order to reduce the effects of gamma rays produced outside the solid angle from the sample to the detector. A lithium fluoride disk is placed in front of the detector to reduce the effect of thermal neutrons scattered by the sample. The detector shielding is shown schematically in Fig. 8.

The final component of the facility is the beam stop, which is used to stop the beam when the shutter is open. The design of this beam stop is very similar to that of the shutter, with the exception that there was considerably more shielding on the front to reduce background levels from radiation scattering back towards the sample.



**Fig. 8** Schematic illustration of the detector shielding

**Fig. 7** Photographs of sample positioning with the sample holder loaded into the sample chamber (a), the brackets which hold the sample holder (b), and the sample holder with a sample loaded using Teflon® film along with the template used to position the samples (c)



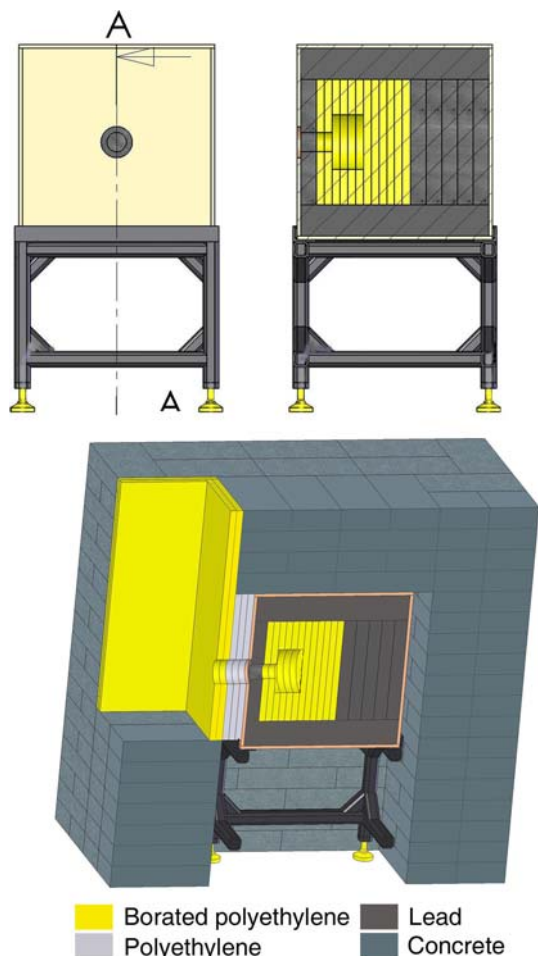


Fig. 9 Schematic illustration of beam stop

Concrete blocks were also stacked around the beam stop to further reduce background radiation levels around the facility. A schematic illustration of the beam stop is presented in Fig. 9.

**Characterization of facility**

**Neutron beam**

The neutron beam for the facility was characterized using BAS-ND neutron sensitive radiograph imaging plates, manufactured by Fujifilm, and gold and nickel foils. The radiographic imaging plates were used to determine the dimensions, shape, uniformity, and location of the neutron beam. The foil measurements were used to measure the thermal and epithermal components of the neutron flux. The measured neutrons fluxes for epithermal and thermal neutrons were  $2.81 \times 10^7 \pm 5.13 \times 10^5$  and  $1.70 \times 10^4 \pm 3.11 \times 10^2 \text{ cm}^{-2} \text{ s}^{-1}$ , respectively. Based on the results of

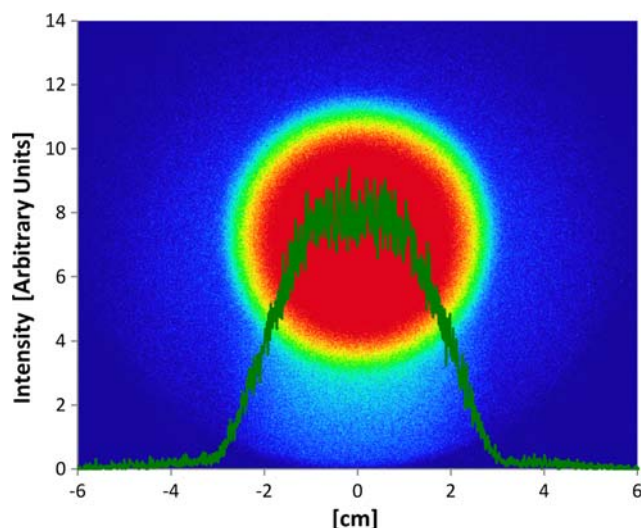


Fig. 10 False-color image and profile of the neutron beam at the sample location with the reactor power at 10 kW. Warmer colors represent highest intensity. The profile plot is a line scan across the horizontal midplane of the image (Color figure online)

the radiograph images, the neutron beam is relatively uniform over a 2-cm diameter at the sample location in the beam center, and the maximum diameter of the beam was approximately 6 cm. The results from the radiograph image taken at the sample location are presented in Fig. 10 along with a plot of the profile across the center of the beam.

**Detector efficiency**

An absolute efficiency curve was obtained for the detector at the sample location, using a combination of calibrated radioactive sources placed in the sample location and PGNAA spectra. The calibrated radioactive sources were used to determine efficiencies below 2 MeV, and the PGNAA spectra for energies greater than 2 MeV. The sources used were  $^{60}\text{Co}$ ,  $^{133}\text{Ba}$ , and  $^{137}\text{Cs}$ . Absolute efficiencies were based on the yields for the emitted gamma energies, and the disintegrations per second, which were calculated from the decay corrected activities. The PGNAA spectra used were Ni, Cl, and Na. The efficiency curve obtained from this analysis is presented in Fig. 11. The efficiency curve was produced by a 5<sup>o</sup> polynomial relating the logarithm of the efficiency to the logarithm of the energy as described by Knoll [10]:

$$\ln(\varepsilon) = \sum a_i \left( \ln \frac{E}{E_0} \right)^{i-1}, \tag{1}$$

where  $\varepsilon$  is the efficiency,  $E$  the energy, and  $E_0$  a reference energy.

**Fig. 11** Absolute efficiency for PGNAA detection system with sample placed in sample chamber and a 60-cm sample to detector distance. The detector used is a 36.50% relative efficient HPGe detector

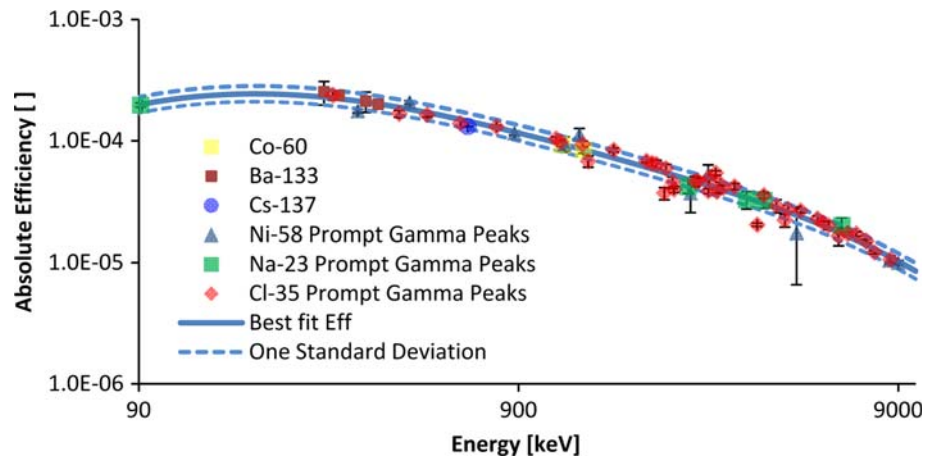
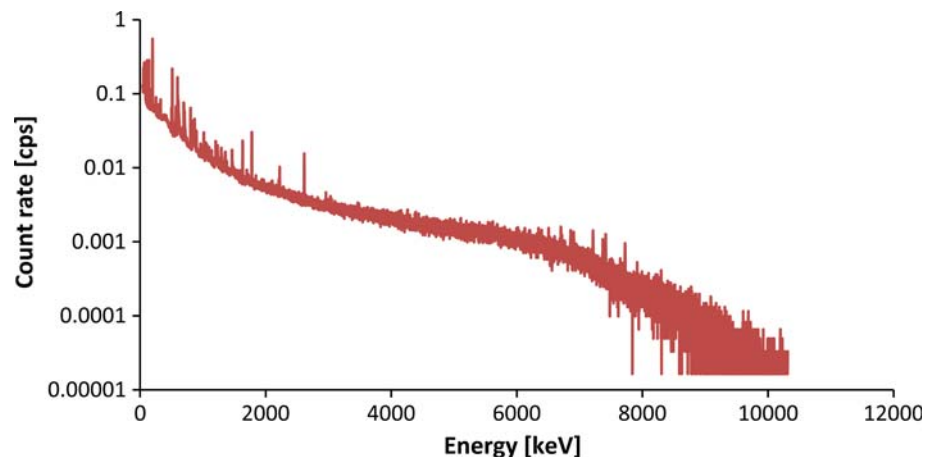


**Fig. 12** PGNAA background spectrum for final shielding configuration, with Teflon<sup>®</sup> sample pouch in place, sample chamber evacuated, reactor power at 1 MW, and with live time of 60,572 s



## Background

After completion of the PGNAA shielding, background spectra were taken to analyze the effectiveness of the neutron and gamma-ray shielding. Some of the results for these measurements are presented in Figs. 12–15. The hydrogen, boron, and lead peaks are present due to the polyethylene, paraffin, borated polyethylene, Boral<sup>®</sup>, and lead shielding in the detector shielding, beam stop, shutter, and biological shield. Aluminum peaks are from the aluminum sample chamber, aluminum beam tubes, aluminum support structure, and the aluminum surrounding the germanium crystal in the detector. Iron peaks are from the steel supporting structure within the facility. Nitrogen is from the air in the sample chamber and is not observed when the chamber is evacuated.

Besides the prominent peaks listed above, there are a large number of prompt and decay germanium peaks, which are a result of neutron interactions within the detector. Some of these are broadened on the high energy side, creating triangular-shaped peaks. Included in these are the peaks at 595.9 and 691.3 keV, which are primarily

a result of the decay of excited  $^{74}\text{Ge}$  and  $^{72}\text{Ge}$  nuclei. These peaks are known as “germanium triangles”, and are from inelastic scattering of fast neutrons within the detector [11].

During the construction of the shielding around the facility, special attention was given to reducing the boron and hydrogen peaks as much as possible. Boron and hydrogen have one of the highest count rates around the facility due to the hydrogen and boron in the shielding material. These elements are also very important from the standpoint of analysis because boron and hydrogen cannot be measured with standard neutron activation analysis techniques. A spectrum with the final shielding configuration and a spectrum before the completion of the lead collimators in the flight tube from the sample to the detector are presented in Figs. 13 and 15. It can be seen from these figures that even though the boron count rate is fairly high due to the boron in the shielding, it was easy to almost completely eliminate it with a small amount of lead because of its low energy. The reduction in the magnitude of the hydrogen peak was not as significant because of its higher energy; however, it was reduced by approximately 30% (Table 2).

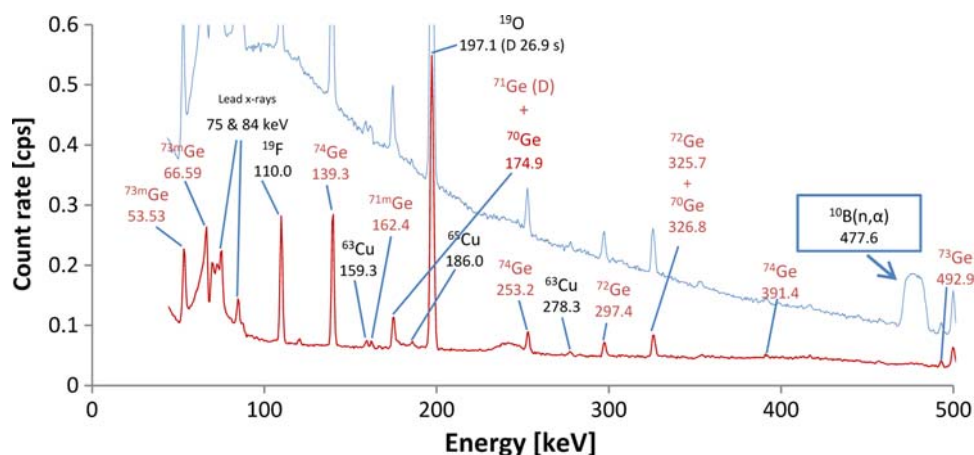
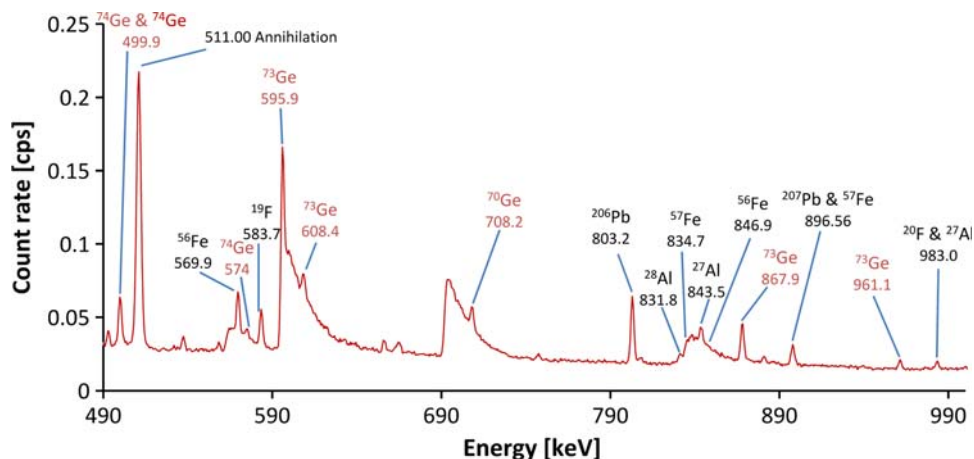


**Fig. 13** PGNAA background spectrum with and without improved detector collimators between 0 and 500 keV. The *blue curve* represents the background before the completion of the detector collimators with a live time of 48,634 s, and the *red curve* represents

the background taken after the completion of the detector collimators with a live time of 60,572 s. Both spectra were taken with the Teflon<sup>®</sup> sample pouch, sample chamber evacuated, and reactor power at 1 MW (Color figure online)

**Fig. 14** PGNAA background spectrum for final shielding configuration between 490 and 990 keV, with Teflon<sup>®</sup> sample pouch, sample chamber evacuated, reactor power at 1 MW, and with live time of 60,572 s



### Sensitivities and detection limits

In order to determine sensitivities and detection limits for some common elements, NIST SRM 1633a coal fly ash, NIST SRM 1571 orchard leaf, and polyethylene samples were analyzed. Sensitivity ( $S$ ) is defined as the counts per second per milligram [ $S = (\text{counts/s})/\text{mg}$ ], and the detection limit was taken to be  $L_d = 3.29\sqrt{R_b}/t/S$ , where  $R_b$  is the background count rate, and  $t$  the count time [12, 13]. The detection limits for these samples are presented in Table 3, and a NIST SRM 1633a coal fly ash spectrum is presented in Fig. 16. These detection limits are approximately a factor of 10–20 less sensitive than the results obtained at the thermal PGNAA facility at NIST [2]. This, however, is to be expected since the NIST reactor is a 20 MW reactor, with a thermal neutron flux of  $3.0 \times 10^8 \text{ cm}^{-2} \text{ s}^{-1}$ , which is about a factor of ten greater than the flux in the facility at the OSTR.

### PGNAA application, analysis of rubidium borodeuteride and sodium borodeuteride

Using the PGNAA facility described above, an analysis was conducted of isotopically labeled rubidium borodeuteride ( $\text{Rb}^{11}\text{BD}_4$ ) and sodium borodeuteride ( $\text{Na}^{11}\text{BD}_4$ ) samples. The borohydrides are of interest as a reversible, light-weight hydrogen storage medium for use with portable fuel-cell applications. In particular, the alkali-metal borohydrides have recently undergone extensive experimental investigation to understand their structural and dynamical properties [14, 15]. For neutron studies, it is important that the borohydrides are synthesized with reactants enriched in  $^{11}\text{B}$  and  $\text{D}$ . An analysis of  $\text{Rb}^{11}\text{BD}_4$  and  $\text{Na}^{11}\text{BD}_4$  samples to be used in upcoming neutron diffraction investigations was performed. The results of the PGNAA investigation, summarized in Table 4, yielded the isotopic abundances of H, D,  $^{10}\text{B}$  and  $^{11}\text{B}$  present in the samples. This information serves



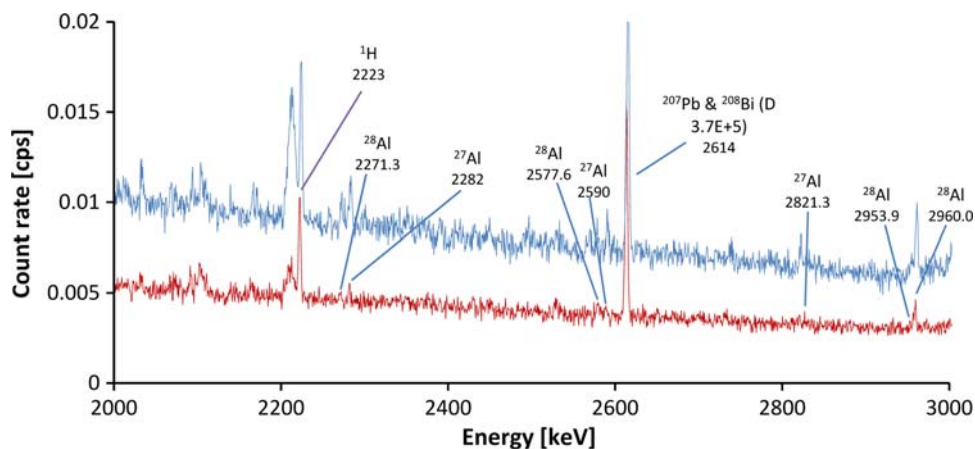


**Fig. 15** PGNAA background spectrum with and without improved detector collimators between 2,000 and 3,000 keV. The *blue curve* represents the background before the completion of the detector collimators with a live time of 48,634 s, and the *red curve* represents

the background taken after the completion of the detector collimators with a live time of 60,572 s. Both spectra were taken with the Teflon<sup>®</sup> sample pouch, sample chamber evacuated, and reactor power at 1 MW (Color figure online)

**Table 2** Count rates for some of the prominent gamma energies in PGNAA background spectra both with and without the sample chamber evacuated for the final shielding configuration

	Energy (keV)	Air in sample chamber Count rate (cps)	Sample chamber evacuated Count rate (cps)
O-19 (D 26.9s)	197.1	1.883 ± 0.009	1.839 ± 0.007
Annihilation	511	1.181 ± 0.008	0.852 ± 0.005
F-19	110	0.489 ± 0.008	0.595 ± 0.006
F	1633.6	0.064 ± 0.003	0.073 ± 0.002
Ge-74	139.3	0.953 ± 0.008	0.663 ± 0.006
Ge	1204.2	0.061 ± 0.004	0.035 ± 0.003
Ge triangle	595.9	2.132 ± 0.026	1.959 ± 0.019
Ge triangle	693	1.282 ± 0.021	1.164 ± 0.016
Ge triangle	1039.5	0.152 ± 0.011	0.107 ± 0.008
B-10	477.6	0.002 ± 0.015	0.028 ± 0.011
Al-27	1014.4	0.073 ± 0.004	0.063 ± 0.002
Al-27 D	1778.9	0.186 ± 0.004	0.111 ± 0.002
Al-27	3034	0.007 ± 0.002	0.003 ± 0.002
Al-27	7213	0.013 ± 0.002	0.007 ± 0.001
H	2223	0.036 ± 0.003	0.025 ± 0.002
207-Pb	803.2	0.165 ± 0.004	0.156 ± 0.003
207-Pb	7368	0.015 ± 0.002	0.004 ± 0.001
Pb & Bi	2614	0.071 ± 0.003	0.067 ± 0.002
Fe	7631 & 7645	0.003 ± 0.003	0.003 ± 0.002
Fe (SE)	7120 & 7134	0.006 ± 0.003	0.0008 ± 0.002
N-14	1678.3	0.023 ± 0.004	Nd <sup>a</sup>
N-14	1884.8	0.048 ± 0.005	0.004 ± 0.002
N (DE)	9807	0.0011 ± 0.0006	Nd <sup>a</sup>

<sup>a</sup> Unable to distinguish from background

as an important input parameter for the analysis of neutron power diffraction rate.

### Conclusions

A versatile PGNAA facility has been built, characterized, and put into operation at the Oregon State University TRIGA<sup>®</sup> reactor. This facility has a thermal neutron flux of  $2.81E + 7$  neutrons/cm<sup>2</sup>/s and a cadmium ratio of 106, as determined by gold foil irradiations. This flux measurement is approximately three times the magnitude of the flux measured at the University of Texas [4], 60% of the flux measured at the Budapest facility [3], and a factor of ten less than the measured flux at the thermal facility at NIST [2]. When scaled by the reactor power, it has sensitivities and detection limits, which are comparable to the thermal PGNAA facility at NIST. In addition to characterization of the facility, it has also been used and demonstrated to be an effective tool in measuring hydrogen and boron concentrations in sodium borodeuteride and rubidium borodeuteride samples on a milligram level. This facility not only will compliment many of the nuclear analysis methods currently used at the Oregon State University TRIGA<sup>®</sup> reactor, but it has also provided means for researchers to analyze substances such as B and H, which could not be detected with the standard instrumental nuclear analysis methods available to them prior to this instrument. Further efforts are ongoing to optimize the shielding of the facility to reduce background levels.

**Table 3** Orchard leaf, coal fly ash, and polyethylene sensitivities

	Mass (mg)	Energy (KeV)	Sensitivity (counts/mg/s)	Detection limit (mg/g)
(1.0213 g sample with 22,363 s count time) NIST SRM 1571 orchard leaf				
B	0.0400 ± 0.007	477	97.1 ± 0.2	(5.6 ± 0.4)E-04
Cl	0.75 ± 0.03	517.07	0.107 ± 0.004	0.27 ± 0.10
Cl	0.75 ± 0.03	785 & 788	0.369 ± 0.015	0.082 ± 0.027
Cl	0.75 ± 0.03	1164	0.228 ± 0.009	0.11 ± 0.05
K	15.0 ± 0.03	770	0.0266 ± 0.005	1.0 ± 0.4
Ca	21.3 ± 0.03	1942	0.0069 ± 0.001	4.6 ± 1.5
(1.015 g sample with 21,122 s count time) NIST SRM 1633a coal fly ash				
B	0.0400 ± 0.0001	477	140 ± 25	(3.1 ± 0.9)E-04
Mg	4.6 ± 0.1	585	0.0408 ± 0.0009	0.56 ± 0.23
Si	231 ± 8	1273	(2.29 ± 0.08)E-04	68 ± 64
Si	231 ± 8	3539	(1.36 ± 0.048)E-03	8.8 ± 7.5
Si	231 ± 8	4934	(8.25 ± 0.029)E-04	12 ± 16
K	19.1 ± 0.6	77	0.028 ± 0.001	0.78 ± 0.27
Ca	11.3 ± 0.1	1942	0.0064 ± 0.0001	2.39 ± 2.24
Ti	8.5 ± 0.1	341.7	0.0685 ± 0.0008	0.40 ± 0.10
Ti	8.5 ± 0.1	1382	0.0703 ± 0.0008	0.28 ± 0.10
Fe	95 ± 1	352	0.0101 ± 0.0001	2.9 ± 0.6
Fe	95 ± 1	7120 & 7135	0.00356 ± 0.00004	2.9 ± 2.7
Fe	95 ± 1	7631 & 7645	0.00269 ± 0.0003	2.2 ± 3.4
Sm	0.016 ± 0.002	334	67.8 ± 8.5	(4.4 ± 1.1)E-04
Gd	0.016 ± 0.002	182	143 ± 19	(2.5 ± 0.5)E-04
Gr	0.016 ± 0.002	1185	13.8 ± 1.8	(1.4 ± 0.7)E-03
(0.1593 g sample with 23,446 s count time) polyethylene				
H	22.753	2223	0.26595 ± 0.00002	0.068 ± 0.011

These values are based on measurements taken with reactor power at 1 MW, and the live times associated with each measurement

**Fig. 16** PGNAA NIST SRM 1633a coal fly ash spectrum, with Teflon® sample pouch, sample chamber evacuated, and reactor power at 1 MW, and with live time of 43,620 s

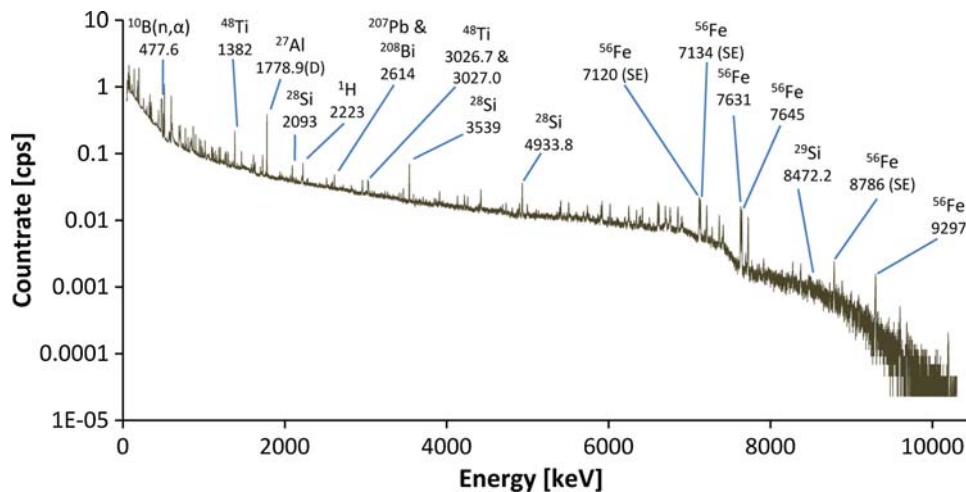


**Table 4** PGNAA borodeuteride results for 0.1037 g Rb<sup>11</sup>BD<sub>4</sub> and 0.1172 g Na<sup>11</sup>BD<sub>4</sub>

Boron-10 (mg)	Hydrogen (mg)	Moles <sup>10</sup> B/ moles <sup>11</sup> B	Moles H/ moles D	Chemical formula	Nominal formula weight of sample (g/mole)
0.397 ± 0.007	0.174 ± 0.020	0.042 ± 0.006	0.045 ± 0.005	Rb <sup>10</sup> B <sub>0.040</sub> <sup>11</sup> B <sub>0.960</sub> H <sub>0.174</sub> D <sub>3.826</sub>	104
1.142 ± 0.020	1.371 ± 0.030	0.042 ± 0.001	0.137 ± 0.003	Na <sup>10</sup> B <sub>0.040</sub> <sup>11</sup> B <sub>0.960</sub> H <sub>0.482</sub> D <sub>3.518</sub>	41.5

**Acknowledgments** We would like to thank the reactor operations staff at the OSTR for working with us to construct, install, and characterize the instrument. We would also like to thank Dr. Gregory Downing at NIST for providing us with the sample chamber for this instrument.

## References

1. Molnár GL, Révay Z, Belgya T, Firestone RB (2000) The new prompt gamma-ray catalogue for PGAA. *Appl Radiat Isot* 53: 527–533
2. Mackey EA, Anderson DL, Liposky PJ, Lindstrom RM, Chen-Mayer H, Lamaze GP (2004) New thermal neutron prompt gamma-ray activation analysis instrument at the National Institute of Standards and Technology Center for neutron research. *Nucl Instrum Methods Phys Res B* 226:426–440
3. Belgya T, Révay Z, Molnar GL (2004) Gamma-ray background at the Budapest PGAA facility. *J Radioanal Nucl Chem* 265:181–191
4. Révey Z, Harrison RK, Alvarez E, Biegalski SR, Landsberger S (2007) Construction and characterization of the redesigned PGNAA facility at the University of Texas at Austin. *Nucl Instrum Methods Phys Res A* 577:611–618
5. Molnar GL (2004) *Handbook of prompt gamma activation analysis*. Kluwer, Boston/London
6. Sueki K, Kobayashi K, Sato W, Nakahara H, Tomizawa T (1996) Nondestructive determination of major elements in a large sample by prompt gamma ray neutron activation analysis. *Anal Chem* 68:2203–2209
7. Adib M, Kilany M (2002) On the use of bismuth as a neutron filter. *Radiat Phys Chem* 66:81–88
8. Shirane G, Shapiro SM, Tranquada JM (2002) *Neutron scattering with a triple-axis spectrometer: basic techniques*. Cambridge, New York
9. Sears VF (1989) *Neutron optics*. Oxford, New York
10. Knoll GF (2000) *Radiation detection and measurement*. Wiley, Michigan
11. Chasman C, Jones KW, Ristinen RA (1965) Fast neutron bombardment of a lithium-drifted germanium gamma-ray detector. *Nucl Instrum Methods* 37:1–8
12. Currie LA (1968) Limits for qualitative detection and quantitative determination. *Anal Chem* 40:586–593
13. Dzuby TG (1977) *X-ray fluorescence analysis of environmental samples*. Ann Arbor Science Publisher INC, Ann Arbor, MI
14. Hartman MR, Rush JJ, Udovic TJ, Bowman RC Jr, Hwang SJ (2007) Structural and vibrational dynamics of isotopically labeled lithium borohydride using neutron diffraction and spectroscopy. *J Solid State Chem* 180:1298–1305
15. Renaudine G, Gomes S, Hagemann, Keller L, Yvon K (2003) Structural and spectroscopic studies on the alkali borohydrides MBH<sub>4</sub> (M = Na, K, Rb, Cs). *J Alloys Compd* 375:98–106